Biophysical Journal, Volume *111*

Supplemental Information

The Effect of Temperature on Microtubule-Based Transport by Cytoplasmic Dynein and Kinesin-1 Motors

Weili Hong, Anjneya Takshak, Olaolu Osunbayo, Ambarish Kunwar, and Michael Vershinin

Supporting Material

Title:

The effect of temperature on microtubule-based molecular motor transport

Authors

W. Hong, A. Takshak, O. Osunbayo, A. Kunwar, M. Vershinin

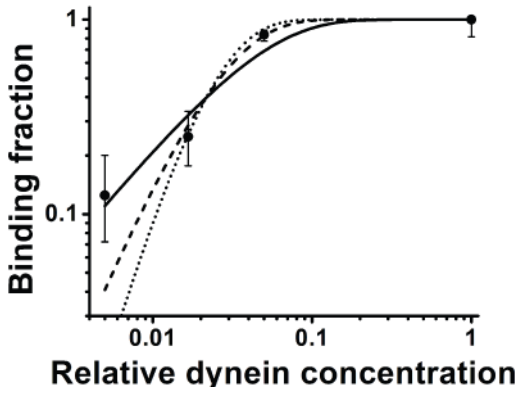

Fig. S1 Single motor activity of cytoplasmic dynein. The binding fraction data for dynein is best fit by single molecule Poisson distribution 1-exp(-n/b) but not by two molecule distribution: 1-exp(-n/b)-(n/b)exp(-n/b) or three molecule distribution 1-exp(-n/b)-(n/b)exp(-n/b))-(n/b)2exp(-n/b)/2 (solid, long dash and short dash curves respectively). Error bars: CI for binomial distribution.

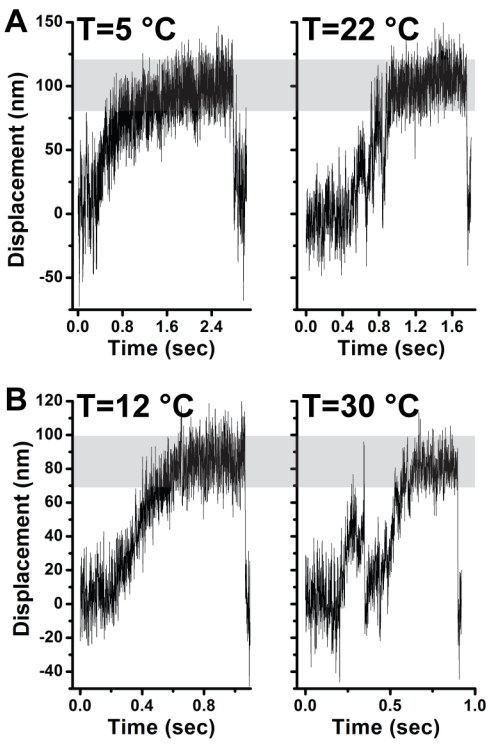

Figure S2. Single motor stalls were experimentally observed for both dynein and kinesin. The stalls were quantified (Fig. 2) for temperatures where motility allowed efficient data collection. Representative examples of motor stall shapes are reported here. Representative stall events for kinesin (A) and dynein (B) motors are shown.

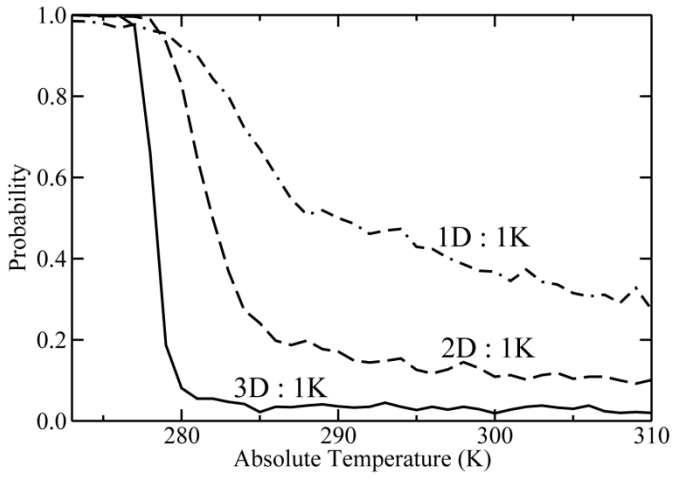

Figure S3. Kinesin “winning probability” for different motor ensembles as a function of temperature. Here, individual dynein (D) and kinesin (K) motor forces were assumed balanced at 2.5 pN. The number of motors in an ensemble is as indicated for each curve. Simulations were performed using the *in-vivo* kinesin-1 and *in-vivo* cytoplasmic dynein parameters given in Text S1 in the Supplementary Material.

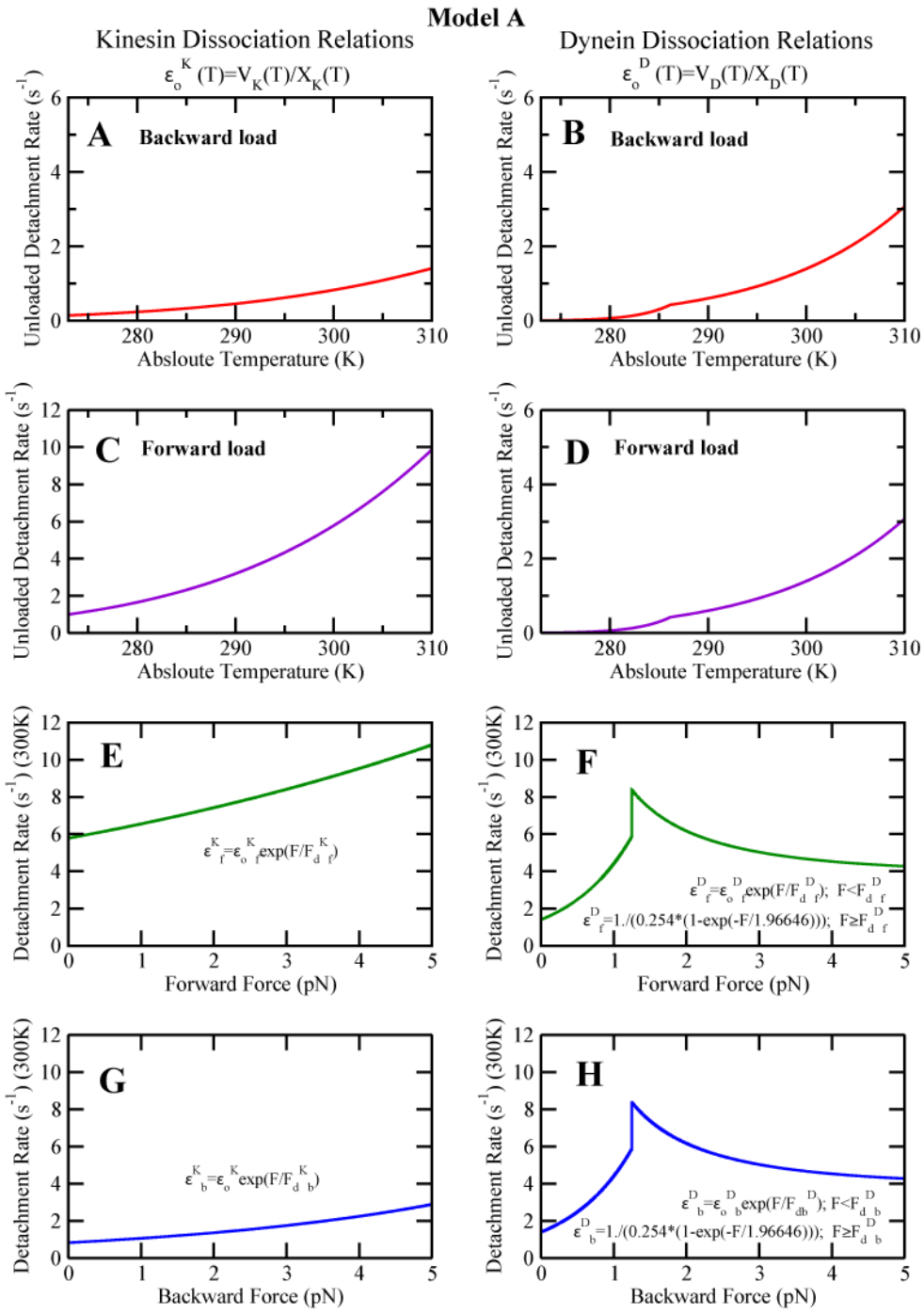

Figure S4. Force- dissociation relations for kinesin-1 and cytoplasmic dynein used in this work for simulations in Fig.3 and the figures in the supplement.

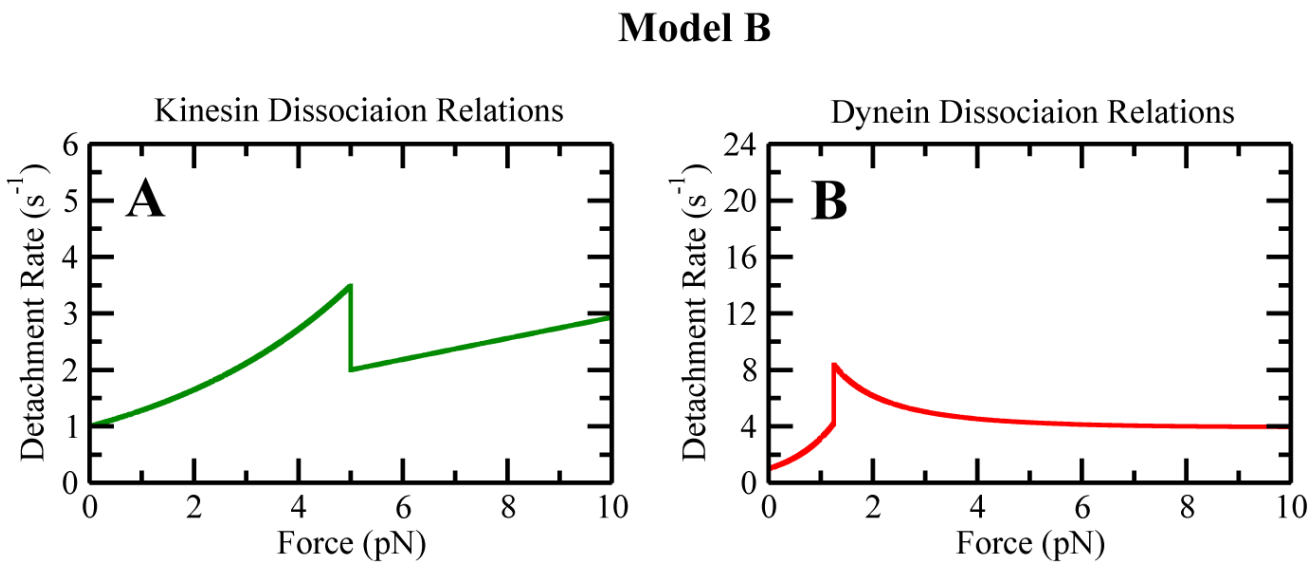

Figure S5: Simulations results in Fig. 4 were performed using detachment kinetics shown in (A) and (B) for Kinesin and Dynein motors respectively.

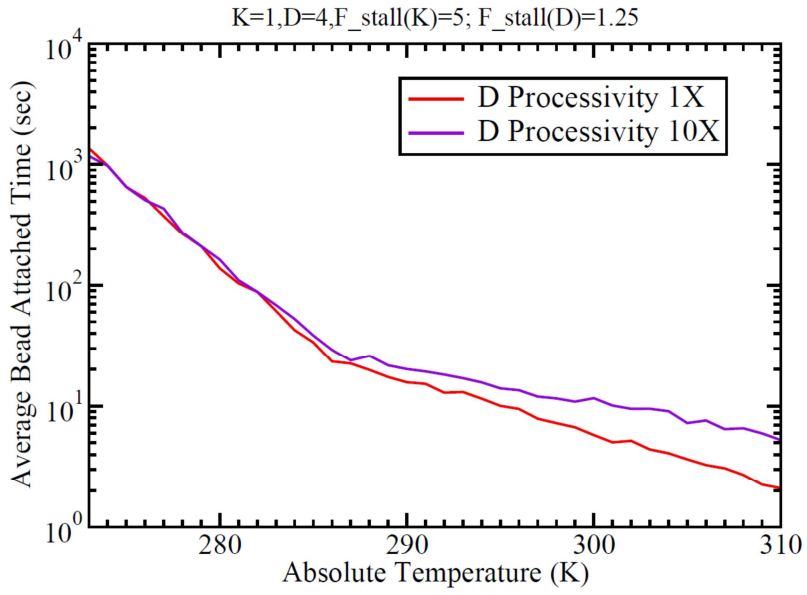

Figure S6. Cargo attachment times show signature of dynein velocity crossover for ensembles of 4 dyneins (1.25 pN stall) and 1 kinesin (5 pN stall) (compare with Fig. 3B). 10X means dynein processivity was increased by a factor of 10.

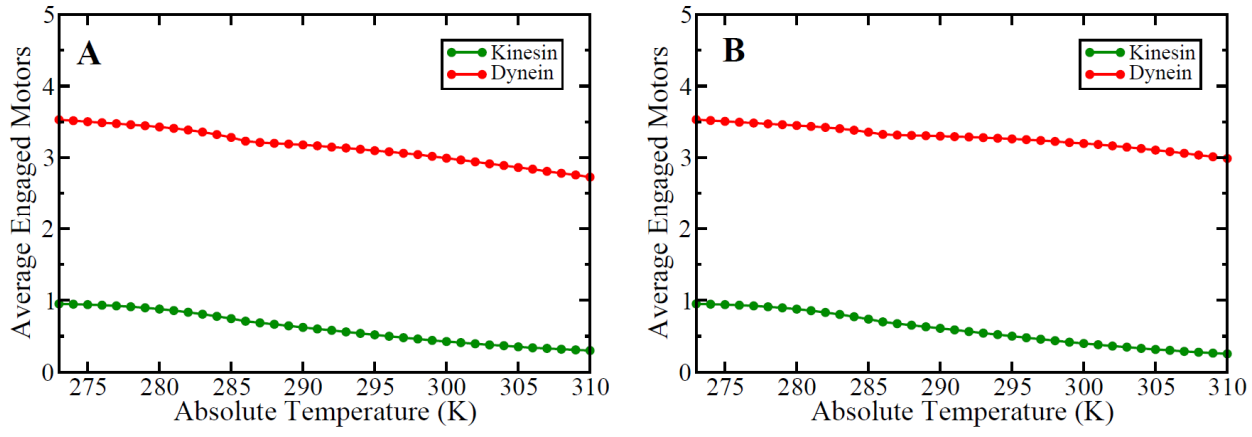

Figure S7. Average ensemble composition for engaged motors. The average number of engaged kinesin and dyneins was calculated for a cargo carrying 4 kinesins and 1 dynein using Model A parameters. We have used 1X (A) and 10X (B) dynein processivity in the simulations but only minor changes at higher temperatures are apparent in the simulated ensembles.

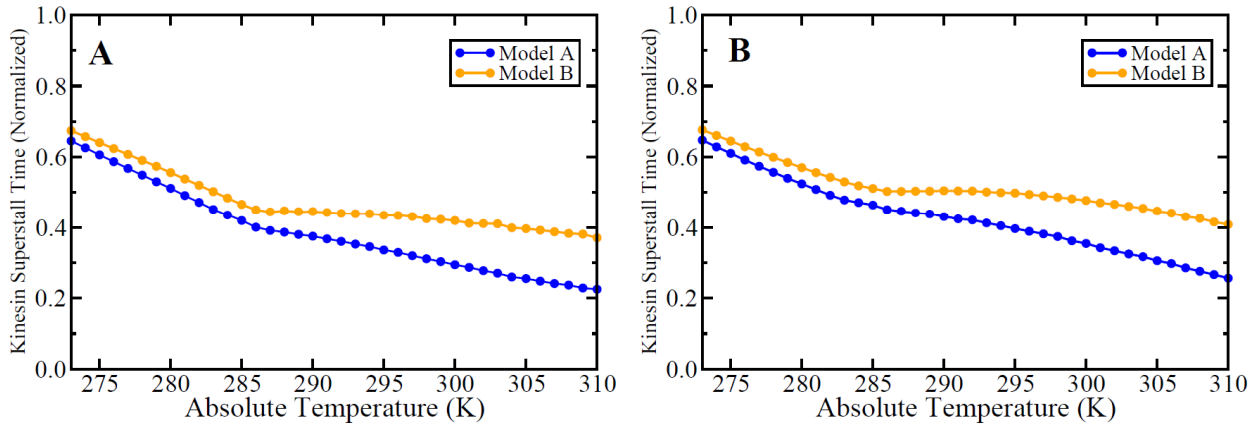

Figure S8. The fraction of time kinesin spends in superstall regime. The gradual decrease in kinesin superstall time fraction as temperature increases is similar for simulations with 1X (A) and 10X (B) dynein processivity.

Movie S1. Simulations of bi-directional transport (Fig. 3) driven by 4 dynein motors and one kinesin at 273 K yielded simulated positions of all motors and the cargo. This data for one representative simulation is shown in movie form (dynein – red, kinesin – green, cargo – black). Motors which are not attached to the MT are not shown so that the number of motors visualized may change from frame to frame.

Movie S2. Simulations of bi-directional transport (Fig. 3) driven by 4 dynein motors and one kinesin at 286 K yielded simulated positions of all motors and the cargo. This data for one representative simulation is shown in movie form (dynein – red, kinesin – green, cargo – black). Motors which are not attached to the MT are not shown so that the number of motors visualized may change from frame to frame.

Movie S3. Simulations of bi-directional transport (Fig. 3) driven by 4 dynein motors and one kinesin at 310 K yielded simulated positions of all motors and the cargo. This data for one representative simulation is shown in movie form (dynein – red, kinesin – green, cargo – black). Motors which are not attached to the MT are not shown so that the number of motors visualized may change from frame to frame.

Text S1.

- **Monte-Carlo Simulation of Temperature Dependent Bi-directional Cargo Motility**

To simulate bidirectional cargo under *in-vitro* and *in-vivo* conditions, we considered a cargo having Kinesin and Dynein motors with various parameters (listed in appropriately labeled Tables later). A Cargo with 'n' Kinesin (Kinesin-1) and 'm' Dynein Motors (Cytoplasmic Dynein) instantaneously attached to the microtubule is abbreviated as (K=n, D=m) in the main text. We used the stochastic model developed by Kunwar *et al.* in [1,2] to simulate the temperature dependence of bidirectional cargo transport by multiple molecular motors of opposing types. The model uses experimentally established parameters for motor function and accurately accounts for many prior experimental results, e.g. the force-velocity curve for kinesin-1[3]. We developed two distinct models to simulate bidirectional cargo motility depending on the detachment kinetics of the involved motors.
In Model A, we considered the anisotropic detachment of Kinesin motors under forward and backward loads measured by Andreasson *et al.* [4], and temperature dependence of unloaded detachment rate of both Kinesin and Dynein motors. While in Model B, we considered isotropic detachment for both sets of motors and used earlier measured detachment kinetics of Kinesin and Dynein motors by Kunwar *et al.* [1].

The common features of both Model A and Model B are briefly described below:

For both models, simulations were performed for temperatures (T) in the range of 273K-310K (0ºC-37ºC) in intervals of 1K. A maximum N number of Kinesin motors and M number of Dynein motors were put on cargo. The motors of both types were modeled as special linkages which exert a restoring force only when they are stretched beyond their rest length and buckle without any resistance when compressed [1,2].The spring constants for both motor types was taken to be k=0.32pN/nm [1,2].The radius of the cargo (r) was taken to be 0.25 µm and the medium viscosity η to be 0.003Pa-s. In our simulations, the velocity of Kinesin and Dynein was dependent on both load felt by the motor, and system temperature.

For both models, Kinesin was considered a simple Arrhenius enzyme whose maximum velocity at zero load (V_o^K) varied with absolute temperature as:

$$V_o^K(T) = A^K * \exp(-E_a^K/(k_B T))$$

Where A^K is the Arrhenius constant for Kinesin; E_a^K is its Activation energy; k_B is Boltzmann Constant and T is the Absolute Temperature. However, Dynein was considered a complex Arrhenius Enzyme because the temperature dependence of its velocity has two distinct domains with two Activation energies: below a critical temperature T_c, Dynein velocity at zero load (V_o^D) is given by

$$V_o^D(T) = A^D * \exp(-E_a^{D1}/(k_B T))$$

While above T_c,

$$V_o^D(T) = A^D * \exp((E_a^{D2} - E_a^{D1})/T_o) * \exp(-E_a^{D2}/(k_B T))$$

Where A^D is the Arrhenius constant for Dynein and E_a^{D1} and E_a^{D2} are its two Activation energies. Kinesin's velocity was considered to reduce sub-linearly with load/ force (F) as

$$V^K(F,T) = V_o^K(T) * (1 - (F/F_s^K)^2)$$

While for dynein, the force-velocity relation was super-linear:

$$V^D(F,T) = V_o^D(T) * (1 - (F/F_s^D)^{0.25})$$

In both models, each simulation was started with all motors attached to the microtubule. Attached Kinesin and Dynein motors start to step along microtubule in opposite directions with stepping rates obtained from force velocity relations i.e. dividing velocity at any given force and temperature by motor step size. Thus motor can get engaged in a tug-of-war if both sets of motors are simultaneously attached to the microtubule. While engaged in a tug-of-war, a motor could experience load in the same or opposite direction of its stepping. It was assumed that forward load had no effect on the motor velocity and only backward load reduced its velocity/stepping rate.

In our models, individual attached motors can either step on the microtubule or detach from the microtubule, at each time step. Conversely, at each time step unattached motors can reattach to the microtubule with re-attachment probabilities determined from their respective on-rates. The cargo continues along the microtubule, instantaneously driven by a number n of engaged Kinesin motors and/or m number of Dynein motors (where $n \leq N$, $m \leq M$ respectively), and is updated at every time step according to motors'

attachment and detachment events, until the simulation ends, or n+m= 0; indicating all motors have fallen off the microtubule.

In our simulations, motor's detachment rate was influenced by both forward as well as backward load. The detachment kinetics of individual type of motors was different in the two models.

In Model A, the unloaded detachment rate of both sets of motors was considered temperature dependent; and was explicitly calculated by dividing the velocity of motors at a particular temperature T by the travel distance (runlength) at that T:

$$\epsilon_o^K(T) = V_o^K(T) / X_o^K(T) \quad (1)$$

Where $V_o^K(T)$ and $X_o^K(T)$ are the unloaded velocity and runlength of Kinesin at a particular temperature T. $X_o^K(T)$ was assumed to be varying exponentially with temperature as:

$$X_o^K(T) = 0.1*\exp(T/32.64)$$

Further, the detachment kinetics of Kinesin was taken to be anisotropic as studied by Andreasson *et al.* [4]. Anisotropic means that the detachment kinetics was different under the influence of forward and backward loads experienced by the motor. A forward load is the one which the motor feels in the same direction as its stepping; while the backward load opposes/hinders motor's stepping. For Kinesin, the detachment kinetics was uniformly exponential throughout for both forward and backward loads [4]. The forward ($F_d^K{}_f$) and backward detachment forces ($F_d^K{}_b$) for Kinesin were considered to be constant (temperature independent) at 8pN [4] and 4pN [1] respectively. Thus the expressions for Kinesin detachment (as a function of both force and temperature) are:

$$\epsilon^K{}_f(F,T)=\epsilon_o^K{}_f(T)*\exp(F/F_d^K{}_f) \quad \text{forward loads (2)}$$

$$\epsilon^K{}_b(F,T)=\epsilon_o^K{}_b(T)*\exp(F/F_d^K{}_b) \quad \text{backward loads (3)}$$

Similarly, the temperature dependence of unloaded detachment rate of Dynein was modeled as:

$$\epsilon_o^D(T) = V_o^D(T) / X_o^D(T) \quad (4)$$

Where the value of $X_o^D(T)$ was taken to be constant at 689 nm. The detachment kinetics of Dynein was considered isotropic as in [1,2], i.e., the detachment kinetics was similar for both forward and backward loads. Also, the detachment kinetics was different for sub-stall and super-stall regimes for both types of loads. The rate of detachment of Dynein motors was taken to be increasing exponentially with load up to stall force (i.e.

$F<F_s^D$ for both forward and backward loads. For loads greater than or equal to single motor stall force experimentally-measured detachment rates were used [1]. The forward ($F_d^D{}_f$) and backward detachment forces ($F_d^D{}_b$) for Dynein were considered to be constant (temperature independent) as for Kinesin; however, their magnitudes were the same at 0.87pN [1,2]. Thus the expressions for Dynein detachment (as a function of both force and temperature) are:

$$\epsilon^D{}_f(F,T)=\epsilon_o{}^D{}_f(T)*\exp(F/F_d^D{}_f) \quad \text{sub-stall forward loads (5)}$$

$$\epsilon^D{}_f(F,T)=1./(0.254*(1.-\exp(-F/1.96646))) \quad \text{super-stall forward loads (6)}$$

$$\epsilon^D{}_b(F,T)=\epsilon_o{}^D{}_b(T)*\exp(F/F_d^D{}_b) \quad \text{sub-stall backward loads (7)}$$

$$\epsilon^D{}_b(F,T)=1./(0.254*(1.-\exp(-F/1.96646))) \quad \text{super-stall backward loads (8)}$$

Plots of equations (1)-(8) are shown in Figure S4. Results obtained from simulation of Model A are shown in Fig 3.

In Model B, the rate of detachment of both Kinesin and Dynein motors was taken to be increasing exponentially with load up to stall force (i.e. $F<F_s^K$ for Kinesin and $F<F_s^D$ for Dynein). Thus, the dependence of Kinesin's and Dynein's detachment rate on force up to stall force is given by

$$\epsilon^K=\epsilon_o{}^K\exp(F/F_d^K) \quad (9)$$

$$\epsilon^D=\epsilon_o{}^D\exp(F/F_d^D) \quad (10)$$

For loads greater than or equal to single motor stall force experimentally-measured detachment rates were used [1]. For Kinesin detachment rate in super-stall regime ($F\geq Fs$) is given by

$$\epsilon^K=1.07+0.186*F \quad (11)$$

for *in-vitro* conditions [1]. Experimentally measured detachment rate of Dynein in super-stall regime [1] is given by

$$\epsilon^D=1./(0.254*(1.-\exp(-F/1.96646))) \quad (12)$$

While the rate of detachment of engaged motor was considered to be dependent on load only, there-attachment/on-rates were taken to be independent of both load and Temperature.

Plots of equations (9)-(12) are shown in Figure S5. Results obtained from simulation of Model B are shown in Fig 4.

Time in each simulation was incremented in discrete time intervals of $\Delta t=10^{-5}$s (time step); since this is appropriately smaller than the rate of the fastest event in our system (viz., the detachment rate of Dynein motor at 310K at $F=F_s^D$). The instantaneous probabilities for motor stepping, detachment and reattachment were calculated by multiplying the respective rates with Δt.

Our simulations included the effect of both thermal noise and the viscous drag. The thermal diffusion of the cargo due to T was assumed to be normally distributed with a mean of $(2D\Delta t)$; where D is the temperature-dependent diffusion coefficient of the cargo [1]. D can be calculated via Einstein's Diffusion relation

$$D = (k_B T)/\gamma$$

Where γ is the drag coefficient of the cargo; which for a spherical cargo is a function of the surrounding medium viscosity (η) and the cargo radius (r) as

$$\gamma=6\pi\eta r$$

At each time step Δt, the net force on the cargo due to all attached motors (say F_{net}) was calculated by the algebraic addition of individual forces exerted by all motors. At each time step Δt, net displacement of the cargo due to motors forces and thermal was obtained by adding displacement X_{drift} caused by F_{net} i.e.

$$X_{drift} = (F_{net}/\gamma)*\Delta t$$

and thermal noise X_{random}; which was drawn from a normal distribution with mean square displacement $(2D\Delta t)$.

The final cargo position (x_f) was obtained after the end of simulation and compared with initial position (x_i). If (x_f-x_i) was positive, then Kinesin was considered to win the Tug-of-War; else Dynein. The above procedure was repeated for 1,000 configurations for each Absolute Temperature from 273K-310K; and the probabilities of motor winning as functions of T were analyzed.

- **Parameters used in Simulations for Model A**

1. *In-vitro* Kinesin-1 Parameters

Parameter	**Symbol**	**Magnitude**
Arrhenius Constant	A^K	1.72448E14 nms^{-1}
Activation Energy	E_a^K	65.05869 kJ/mol
Spring Constant	k_K	0.32 pN/nm
Rest Stalk Length	L_K	110 nm
Step size	d_K	8 nm
Stall Force	F_s^K	5.00 pN
Forward Detachment Force	$F_d{}^K{}_f$	8.00 pN
Backward Detachment Force	$F_d{}^K{}_b$	4.00 pN
Rate of attachment	π^K	5 s^{-1}

2. *In-vitro* Cytoplasmic Dynein Parameters

Parameter	**Symbol**	**Magnitude**
Arrhenius Constant	A^D	1.68497E39 nms^{-1}
Critical Temperature	T_C^D	286.1722 K
Activation Energy for $T<T_C^D$	E_a^{D1}	201.3638 kJ/mol
Activation Energy for $T\geq T_C^D$	E_a^{D2}	60.9441 kJ/mol
Spring Constant	k_D	0.32 pN/nm
Rest Stalk Length	L_D	50 nm
Step size	d_D	8 nm
Stall Force	F_s^D	1.25 pN
Forward Detachment Force	$F_d{}^D{}_f$	0.87 pN
Backward Detachment Force	$F_d{}^D{}_b$	0.87 pN
Rate of attachment	π^D	5 s^{-1}
Unloaded Runlength	X_o^D	689 nm

3. *In-vivo* Kinesin-1 Parameters

Parameter	**Symbol**	**Magnitude**
Arrhenius Constant	A^K	1.72448E14 nms^{-1}
Activation Energy	E_a^K	65.05869 kJ/mol
Spring Constant	k^K	0.32 pN/nm
Rest Stalk Length	L_K	110 nm
Step size	d_K	8 nm
Stall Force	F_s^K	2.50 pN
Forward Detachment Force	$F_d{}^K{}_f$	8.00 pN
Backward Detachment Force	$F_d{}^K{}_b$	2.00 pN
Rate of attachment	π^K	5 s^{-1}

4. *In-vivo* Cytoplasmic Dynein Parameters

Parameter	**Symbol**	**Magnitude**
Arrhenius Constant	A^{D}	1.68497E39 nms^{-1}
Critical Temperature	To	286.1722 K
Activation Energy for T<To	E_a^{D1}	201.3638 kJ/mol
Activation Energy for T≥To	E_a^{D2}	60.9441 kJ/mol
Spring Constant	k_D	0.32 pN/nm
Rest Stalk Length	L_D	50 nm
Step size	d_D	8 nm
Stall Force	F_s^{D}	2.50 pN
Forward Detachment Force	$F_d^{D}{}_f$	1.74 pN
Backward Detachment Force	$F_d^{D}{}_b$	1.74 pN
Rate of attachment	π^{D}	5 s^{-1}
Unloaded Runlength	X_o^{D}	689 nm

- **Parameters used in Simulations for Model B**

1. *In-vitro* Kinesin-1 Parameters

Parameter	**Symbol**	**Magnitude**
Arrhenius Constant	A^K	1.72448E14 nms^{-1}
Activation Energy	E_a^K	65.05869 kJ/mol
Spring Constant	k_K	0.32 pN/nm
Rest Stalk Length	L_K	110 nm
Step size	d_K	8 nm
Stall $_F$orce	F_s^K	5.00 pN
Detachment Force	F_d^K	4.00 pN
Rate of attachment	π^K	5 s^{-1}
Rate of detachment at zero load	ϵ_o^K	1 s^{-1}

2. *In-vitro* Cytoplasmic Dynein Parameters

Parameter	**Symbol**	**Magnitude**
Arrhenius Constant	A^D	1.68497E39 nms^{-1}
Critical Temperature	T_C^D	286.1722 K
Activation Energy for $T<T_C^D$	E_a^{D1}	201.3638 kJ/mol
Activation Energy for $T\geq T_C^D$	E_a^{D2}	60.9441 kJ/mol
Spring Constant	k_D	0.32 pN/nm
Rest Stalk Length	L_D	50 nm
Step size	d_D	8 nm
Stall Force	F_s^D	1.25 pN
Detachment Force	F_d^D	0.87 pN
Rate of attachment	π^D	5 s^{-1}
Rate of detachment at zero load	ϵ_o^D	1 s^{-1}

3. *In-vivo* Kinesin-1 Parameters

Parameter	**Symbol**	**Magnitude**
Arrhenius Constant	A^K	1.72448E14 nms^{-1}
Activation Energy	E_a^K	65.05869 kJ/mol
Spring Constant	k^K	0.32 pN/nm
Rest Stalk Length	L_K	110 nm
Step size	d_K	8 nm
Stall Force	F_s^K	2.50 pN
Detachment Force	F_d^K	2.00 pN
Rate of attachment	π^K	5 s^{-1}
Rate of detachment at zero load	ϵ_o^K	1 s^{-1}

4. *In-vivo* Cytoplasmic Dynein Parameters

Parameter	**Symbol**	**Magnitude**
Arrhenius Constant	A^D	1.68497E39 nms^{-1}
Critical Temperature	To	286.1722 K
Activation Energy for T<To	E_a^{D1}	201.3638 kJ/mol
Activation Energy for T≥To	E_a^{D2}	60.9441 kJ/mol
Spring Constant	k_D	0.32 pN/nm
Rest Stalk Length	L_D	50 nm
Step size	d_D	8 nm
Stall Force	F_s^D	2.50 pN
Detachment Force	F_d^D	1.74 pN
Rate of attachment	π^D	5 s^{-1}
Rate of detachment at zero load	ϵ_o^D	1 s^{-1}

- **References**

1. Kunwar A., Tripathy S.K., Xu J., Mattson M.K., Anand P., Sigua R., Vershinin M., McKenney R., Yu C.C., Mogilner A. and Gross S.P. (2011) Mechanical Stochastic Tug-of-War Models cannot explain Bidirectional Lipid-droplet Transport: *PNAS 108:*18960-18965.

2. Kunwar A., Vershinin M., Xu J. and Gross S.P. (2008) Stepping, Strain-Gating andan Unexpected Force-Velocity curvefor Multiple-Motor-Based Transport: *Current Biology 18:*1173-1183.

3. Schnitzer M.J., Visscher K., Block S.M. (2000) Force production by single kinesin motors. *Nat Cell Biol.* 2:718–723.

4. Andreasson J.O.L., Milic B., Chen G.Y., Guydosh N., Hancock W.O., Block S.M. (2015) Examining kinesin processivity within a general gating framework: eLife 2015:e07403.